Three Dimensional Identification of Zonal Flows in the HL-2A Tokamak

L.W. Yan 1), W.Y. Hong 1), T. Lan 2) K.J. Zhao 1), J.Q. Dong 1), A.D. Liu 2),
C.X. Yu 2), J. Qian 1), J. Cheng 1), D.L. Yu 1), Y. Huang 1),
Q.W. Yang 1), X.T. Ding 1), Y. Liu 1), and C.H. Pan 1)

1) Southwestern Institute of Physics, Chengdu 610041, China
2) Department of Modern Physics, University of Science and Technology of China, Hefei 230026, China
The e-mail address of main author: lwyan@swip.ac.cn

Abstract A novel design of three-step Langmuir probe (TSLP) array has been developed for zonal flow (ZF) studies in the HL-2A tokamak. Three TSLP arrays are used to determine three dimensional (3-D) features of zonal flows. Two arrays have poloidal separation of 6.5 cm, while the third array is toroidally separated by 80 cm. The TSLP structure is described in detail. The 3-D properties of geodesic acoustic mode (GAM) ZFs are analyzed. The poloidal and toroidal mode numbers (m<1/n~0) of radial electric field perturbations are simultaneously determined in the HL-2A tokamak for the first time. The modes have narrow radial wave numbers ($k_r\rho_i =$ 0.03-0.07), corresponding to radial scale lengths of 2.4-4.2cm. High coherence of both the GAM and the ambient turbulence separated by toroidal 22.5 degree along a magnetic field line is observed, in contrast with the high coherence of the GAM but low coherence of the ambient turbulence apart from the same field line. The nonlinear three wave coupling between the high frequency turbulent fluctuations and the flows is a plausible mechanism of the flow generation.

1. Introduction

Zonal Flows (ZFs) are ubiquitous in space and laboratory plasmas. Recently, a comprehensive review about the ZF physics, including its theory, numerical simulation and experiment results, has been finished [1]. The main goal for the ZF study is understanding turbulent transport and improving plasma confinement in magnetic fusion devices. Theoretical researches indicate turbulence can induce plasma transport and create coherent ZFs, which reversely regulate the former [2]. Two kinds of zonal flows have been predicted in magnetic confinement plasmas, including the near zero low frequency zonal flow (LFZF) and the geodesic acoustic mode zonal flow (GAMZF). There are poloidal and toroidal symmetries (m = 0 / n = 0) for the two kinds of ZFs. The GAMZF has a frequency of $f_{GAM}^{th} \sim \left(\sqrt{(T_e+T_i)/M_i}/2\pi R\right)(1+1/2q^2)$ and collisionless damping rate of $\gamma_L \sim \omega \exp(-\alpha q^2)$. Here R, q, α are major radius, safety factor, and a coefficient of order unity. The other parameters have normal meanings. The ZF has longer autocorrelation time $\tau_{ac} = \left(\Delta\omega_{ZF}\right)^{-1}$ and smaller rotation speed $V_{ZF} \sim 10^{-2} V_{th,i}$ than ambient turbulence. It exists over a wide region inside the last closed flux surface (LCFS).

Zonal Flows have been studied in many fusion devices using different diagnostic techniques. For example, the GAM with the frequency of $f_{GAM} \sim$ 15 kHz, poloidal mode number (m<3) and radial wave number ($k_r\rho_i \sim 0.2$) is observed in the DIII-D tokamak [3]. The GAM behaviors and scaling dependence are further discussed [4, 5]. The radial and poloidal features of the GAM oscillations are also studied in ASDEX Upgrade [6]. Two types of coherent electrostatic modes (f ~1 kHz and 10-12 kHz) with small poloidal wave numbers are obtained in the JFT-2M tokamak [7]. Moreover, the GAM features are further investigated through direct and simultaneous measurements of electrostatic and density fluctuations [8]. The GAMs in the T-10 tokamak are investigated as well [9]. They are found to have density

limit and magnetic components, and more easily excited near low q rational surfaces. The poloidal distribution of density fluctuation induced by the GAM is measured in the TEXTOR tokamak [10]. The poloidally long wavelength flows relevant to the ZF is reported in the HT-7 tokamak [11]. The strong reduction in fluctuation-driven particle flux in the presence of zonal flows is observed from H-1 toroidal heliac [12]. The toroidal structure of zonal flow is only observed on the Compact Helical System [13] with toroidal mode number of n~0. It has not been reported from a tokamak. Especially, simultaneous determination of poloidal and toroidal features of ZFs has never been conducted in a fusion device. Recently, a novel design of the TSLPs has been successful applied to the 3-D zonal flow studies in the HL-2A tokamak [14]. This paper presents the GAMZF measurement results in the HL-2A tokamak in detail. The remainder of this paper is arranged as follows. Section 2 presents the arrangement of three-step Langmuir probe arrays. The experimental methods for zonal flows are described in Sec.3. Experimental results about zonal flows are given in Sec. 4. Section 5 is for the conclusions.

2. The Arrangement of Three-Step Langmuir Probe Arrays

A novel TSLP array is first designed to measure the 3-D features for the ZFs. Figure 1 shows the structure of the array used in the HL-2A tokamak. Each array composes of 6 tips possessing 4 mm separation between two steps. Each tip has a diameter of 1.5 mm and protrudes 2 mm above a step. The sizes of probe array are denoted in figure 1, which is described by Reference [15] in detail. During the ZF experiments, tips 1-5 are used to measure floating potential, while tip 6 measures ion saturation current. The averaged poloidal angle between tip 2 (4) and 3 (5) has the same poloidal angle as tip 1, which avoids locating tips 2 and 3 in the shadow region of tip 1 along a magnetic field line.

Two TSLP arrays forming a set of 10 tips (named 1-10) are placed in the same toroidal position with a poloidal separation of 6.5 cm, while the third TSLP array of electromotive 6 probes (numbered 11-16) is separated toroidally by 80 cm or with the toroidal angle 22.5^0, as shown in figure 2. The tip 6 is not applied in the arrays 1 and 2 due to the limitation of extraction wires. Both the 10 probe set and the third array are mounted at the outboard midplane of the tokamak with up-down symmetry. The novel design of three steps may ensure the poloidal and toroidal correlation coefficients of different arrays to have large values through optimizing the tip choice of adjacent steps. A fourth TSLP array driven by pneumatically reciprocating system is applied to measure edge electron temperature and density profiles with toroidal separation of 210 cm or toroidal angle of 60^0 [16]. The poloidal separation of 10 probe set can be chosen as 6.5, 9.0 or 9.5 cm. In order to ensure tip 1 (6) and 11 at the same magnetic field line, the edge safety factor ($q(r) = \Delta\phi / \Delta\theta$) at the LCFS should be 4.8, 3.5 and 3.3 after toroidal angle is fixed at $\Delta\phi = 22.5^0$ for the three separations as above.

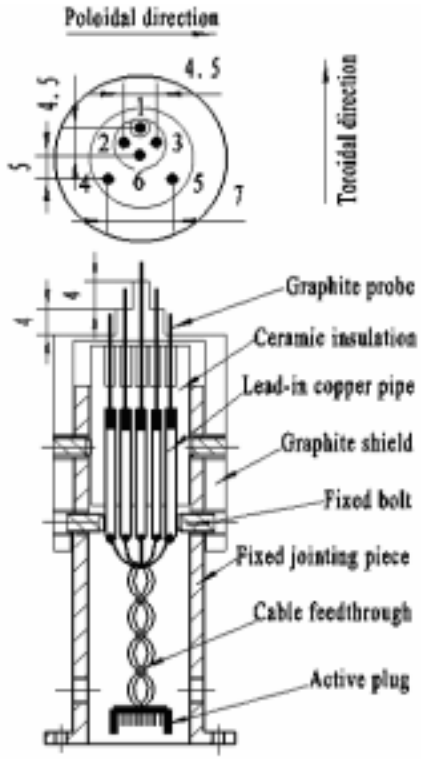

FIG.1. The structure of the three step Langmuir probe array for zonal flow study in the HL-2A tokamak

There is a maximum value for toroidal coherency if tips 1 and 11 are at the same field line. The radial positions of all the TSLP arrays can be adjusted in the interval between discharges. Such an arrangement as shown in figure 2 allows us to make 3-D direct measurements of floating potential at plasma edge and to calculate the profiles of radial electric field. Three electric fields are used in this paper. They are defined as $E_{r1} = (\phi_{f1} - (\phi_{f2} + \phi_{f3})/2)/\delta r$, $E_{r2} = (\phi_{f6} - (\phi_{f7} + \phi_{f8})/2)/\delta r$ and $E_{r3} = (\phi_{f11} - (\phi_{f12} + \phi_{f13})/2)/\delta r$, where $\delta r = 4\ mm$ is step separation. The float potentials of tips 1 -16 are named $\phi_{f1} - \phi_{f16}$. The novel design of the TSLP array has very good flexibility to measure 3-D properties of the zonal flows.

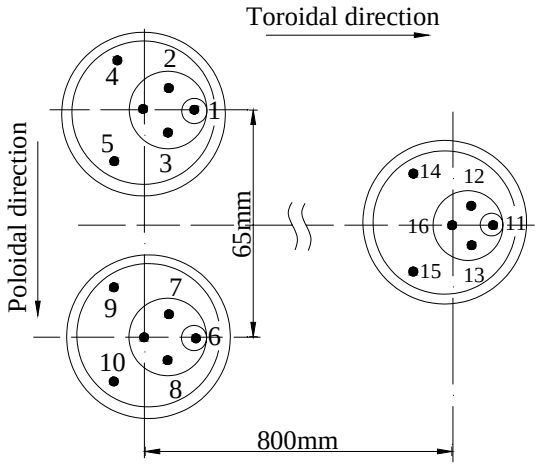

FIG. 2. The arrangement of three TSLP arrays for 3-D zonal flow study in HL-2A

Tips 1-10 are used for the poloidal ZF coherency, while the toroidal ZF coherency is combined tips 1-10 with tips 11-16.

3. The Experimental Methods for Zonal Flows

HL-2A is a middle size tokamak with double null closed divertor. The main designed parameters are, major radius R = 1.65 m, minor radius a = 0.40 m, plasma current Ip = 480 kA, Bt = 2.8 T and discharge duration for 4 s [17]. Recent achieved parameters are, R = 1.65 m, a = 0.40 m, Ip = 400 kA, Bt = 2.65 T, line averaged density $n_{el} = 5.5\times10^{19}$ m^{-3} and discharge duration for 2.96 s. The typical parameters for ZF experiments are, R = 1.65 m, a = 0.40 m, Ip = 200-350 kA, Bt = 2.2-2.5 T, n_{el} = (1-3) $\times10^{19}$ m^{-3} and discharge plateau duration for 0.2-1.0 s. The current and magnetic field directions are counter-clockwise. High safety factor (q_a ~ 5.0) discharges are desirable for avoiding MHD instability. Limiter configuration discharge with hydrogen fuelling is chosen for determining minor radius precisely.

Reference [16] introduces the probe measurement system in detail. The response frequency of probe circuit is higher than 500 kHz, the phase error is less than 2^0 at 500 kHz. All signals are acquired with the frequency of 1 MHz at the accuracy of 12 bits, the corresponding Nyquist frequency of FFT analysis is $f_N = 500$ kHz. The number realized ensemble average is 200 using 2^{11} data records each with half data overlap, the frequency resolution is 0.49 kHz in the following ZF analysis. The conventional principles and schemes are applied to our correlation analyses [13, 18]. The electric field perturbations are used for the correlation analyses in this paper unless otherwise stated.

4. Experimental Results about Zonal Flows

The GAMZFs have not been observed if the probe arrays are located outside of the LCFS. They begin to appear at the position of 1 cm inside the LCFS in HL-2A and have large perturbation amplitude near 3 cm inside the LCFS. So far, the LFZF is still under analyses. Two discharges with the GAMZFs have been analyzed in detail. One has higher safety factor than the other. The autopower spectra of the two discharges are shown in figure 3. Main

parameters for the two GAM discharges are listed in Table 1. Here ρ_i is the ion Larmor radius, T_e is the electron temperature at the ZF region. The GAM frequencies at peaks are 9.3 kHz for shot 4044 and 6.8 kHz for shot 4206, respectively. The frequencies predicted by theory are $f_{GAM}^{th} = 8.5kHz$ and 5.8 kHz using T_e = 38 eV and 17 eV, respectively, assuming $T_i = T_e$. The scaling dependence of $f_{GAM}^{th} \approx 0.88 f_{GAM}$ indicates that the results of theory and experiment are in good agreement. The safety factors are decreased to ~$0.88q_a$ at the position of normalized radius r/a = 0.93. The full width of half magnitude (FWHM) for the GAMZF peak is 3-5 kHz, corresponding to the lifetime of 0.2-0.3 ms. The lifetime is over 20 times of the turbulent decorrelation time with an order of magnitude $\tau_d \sim 10\mu s$. The radial and poloidal correlation lengths of ambient turbulence are estimated as 1 cm and 2 cm, respectively. Both are much shorter that the corresponding scale lengths of GAMZFs.

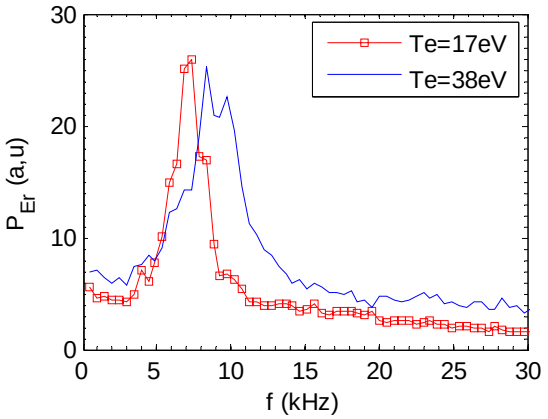

FIG.3. The auto-power spectra with the GAMZFs for shots 4044 and 4206.

The GAM frequencies at peaks are 9.3 kHz for shot 4044 and 6.8 kHz for shot 4206, respectively.

TABLE I MAIN PARAMETERS OF THE TWO GAMZF DISCHARGES

shot	r/a	I_p (kA)	n_{el} ($10^{19}m^{-3}$)	q_a	ρ_i (mm)	T_e (eV)	f_{GAM} (kHz)
4044	0.93	200	2	5.3	0.27	38	9.3
4206	0.92	300	2.5	3.5	0.18	17	6.8

This paper is focused on the 3-D spatial structure of the GAMZFs. Figure 4 presents the poloidal coherencies for the two discharges. Shown here are (a) poloidal coherency spectra of E_{r1} and E_{r2}, (b) the poloidal phase differences $\Delta\phi_\theta$ between E_{r1} and E_{r2}, and (c) the poloidal wave vectors k_θ versus frequency estimated from ϕ_{f2} and ϕ_{f3}. The coherencies of 0.6 for shot 4044 and 0.79 for shot 4206 in the GAM frequency region clearly indicate the strong poloidal correlation of the fluctuations over the poloidal distance *of* d_θ = 6.5 cm, which is much longer than the poloidal correlation length of the ambient turbulence (~2 cm) estimated as above. The dashed line gives the uncertainty level (~0.07) in the coherency spectra.

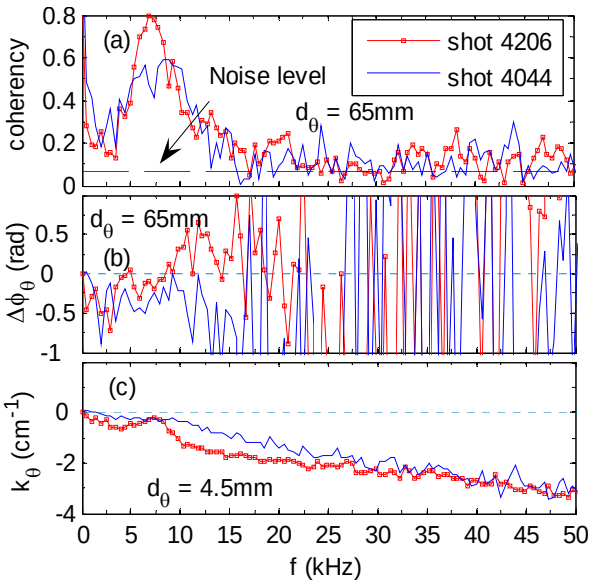

FIG. 4. Poloidal coherencies for the two GAMZF discharges

(a) The poloidal coherency spectra of E_{r1} and E_{r2}, (b) the poloidal phase differences $\Delta\phi_\theta$ of E_{r1} and E_{r2}, and (c) the poloidal wave vectors k_θ via frequency using the potentials of tips 2 and 3.

The phase differences at the GAM frequencies are $\Delta\phi_\theta = -0.173$ for shot

4044 and -0.096 for shot 4206, as shown in figure 4(b). On average within the width of half maximum, the poloidal wave vectors of the GAMZFs are $k_\theta = -0.05 \pm 0.03$ and $k_\theta = -0.02 \pm 0.01$ cm^{-1} for the two shots, respectively. The poloidal mode numbers are estimated as *m~1.8* and *m~0.7*. The poloidal wave vector k_θ versus frequency estimated from ϕ_{f2} and ϕ_{f3} is illustrated in figure 4(c). Here the general dispersion relations of the ambient turbulence, straight lines without offsets due to the short distance ($d_\theta = 0.45cm$) between the two tips, are deviated in the GAM frequency region. The ambient turbulences propagate in the electron diamagnetic drift direction. The mode number difference from theory (m = 0) will be discussed later.

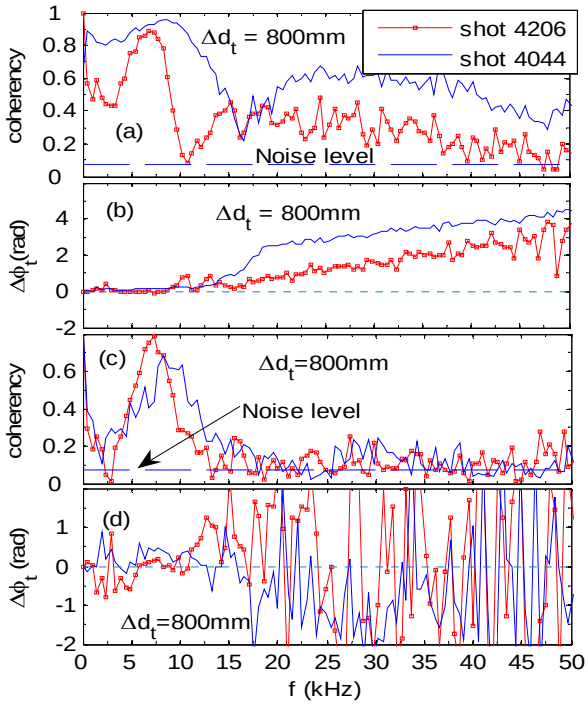

FIG.5. Toroidal coherencies for the two GAMZF discharges

(a) The toroidal coherency spectra of E_{r1} and E_{r3}, (b) the phase differences $\Delta\phi_t$ between E_{r1} and E_{r3}, (c) the toroidal coherency spectra of E_{r2} and E_{r3}, and (d) the phase differences $\Delta\phi_t$ between E_{r2} and E_{r3}.

The toroidal coherencies of the radial electric field perturbations are shown in figure 5. Presented here are (a) the toroidal coherency spectra of E_{r1} and E_{r3}, (b) the phase differences $\Delta\phi_t$ between E_{r1} and E_{r3}, (c) the toroidal coherency spectra of E_{r2} and E_{r3}, and (d) the phase differences $\Delta\phi_t$ between E_{r2} and E_{r3}. The dashed lines in figure 5(a) and 5(c) are still the uncertainty level in the coherency spectra. The connection line from the tip *1* to *11* is almost parallel to the magnetic field line for the two shots, especially for shot 4044. The strong toroidal correlations at the GAM frequency over the d_t = 80 cm distance are proved by the coefficients of 0.96 for shot 4044 and 0.90 for shot 4206. The sharp decreases of the phase difference in the GAM frequency region noticeably distinguish the GAMZFs from the ambient turbulence. The toroidal wave vectors are $k_\phi = (0.22 \pm 0.04) \times 10^{-2}$ cm^{-1} and $k_\phi = (0.02 \pm 0.07) \times 10^{-2}$ cm^{-1} in the GAMZF frequency region for the two shots. The corresponding toroidal mode numbers are $n = 0.33 \pm 0.0.07 \sim 0$ and $n = 0.0 \pm 0.1 \sim 0$. We note that the coherencies of the ambient turbulence in middle frequency region (20<*f* <50 kHz) are lower than those of the GAMZFs but comparable (especially for shot 4044). In addition, the phase shifts in Fig. 5(b) exhibit clearly linear dispersion relations in that region. These results indicate that the ambient turbulence has also coherence over the 80 cm distance along the field line from tip 1 to 11. The correlation length of drift wave turbulence is long along the field line. Therefore, the coherencies in the frequency region of the ambient turbulence are not very low for this set of data.

In order to further verify this idea, the coherencies between E_{r2} and E_{r3} are examined and the results are given in figure 5(c) and 5(d). There is a small angle between the connection line from probe tip 6 to 11 and the field line, which is ~9.8^0 for shot 4044 and ~12.1^0 for shot 4206. Here the coherencies of the GAMZFs are 0.69 for shot 4044 and 0.79 for shot 4206, respectively. The toroidal wave vectors in the GAMZF frequency region are

$k_\phi = (0.4 \pm 0.1) \times 10^{-2}$ and $k_\phi = (0.1 \pm 0.2) \times 10^{-2}$ cm^{-1}, corresponding to toroidal mode numbers $n = 0.7 \pm 0.2 \sim 1$ and $n = 0.2 \pm 0.3 \sim 0$. The important difference is that the coherencies are lower than 0.2 and no clear linear dispersion relations are observed for the ambient turbulence of this set of data. The physics reason is that the field line length from probe tip 11 and 6 is much longer than 80 cm or the correlation length. The similarity and the sharp contrast of the coherencies and the phase shifts between two data sets in the GAM and turbulence frequency regions confirm that the observed oscillations of the GAM frequency are zonal flows with toroidal mode number *n~0.*

The TSLP array is rather convenient to observe the radial features of the electrostatic and electric field perturbations. Figure 6 presents the radial coherencies for the two discharges. Given here are (a) the radial coherency spectra of ϕ_{f1} and $(\phi_{f2} + \phi_{f3})/2$, and (b) the corresponding radial wave vector k_r versus frequency. There are the maximum coherent coefficients near the GAMZF frequencies, which are 0.78 for shot 4044 and 0.98 for shot 4206, respectively. Strong correlation is observed for ambient turbulence in the separation of 4 mm with the frequency f < 50 kHz. The standard dispersion relations for the ambient turbulence are also reproduced except the GAMZF regions. The radial wave vectors significantly increase in the GAMZF frequency region, indicating much localized structure of the zonal flows. After the contribution of ambient turbulence with the short wavelength is filtered, the more accurate radial wave vectors at the peak frequencies are calculated from ϕ_{f1} and ϕ_{f7} as $k_r = 2.6 \pm 0.2$ cm^{-1}for shot 4044 and $k_r = 1.5 \pm 0.2$ cm^{-1} for shot 4206, corresponding to the radial scale lengths of $\lambda = 2.4$ or 4.2 cm for the two discharges. Both have narrow radial extents of $k_r \rho_i = 0.07$ and 0.03. The shear rate of the GAMZF can be estimated as $\gamma_{ZF} = k_r v_{\theta ZF} \sim 4 \times 10^4 / s$ for shot 4206, which is lower than but comparable with the decorrelation rate of the ambient turbulence $\tau_{AT} \sim 1/\tau_d = 10^5 / s$. This shear rate of the GAMZF is not enough to suppress the ambient turbulence, but the latter can be regulated by the former rather largely.

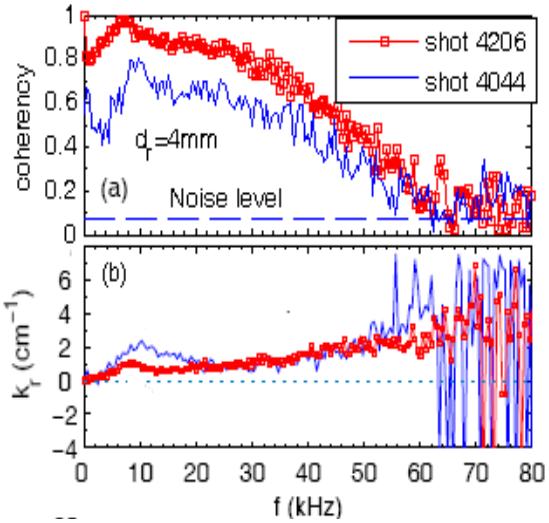

FIG.6. Radial coherencies for the two GAMZF discharges

(a) The radial coherency spectra of ϕ_{f1} and $(\phi_{f2} + \phi_{f3})/2$, and (b) the radial wave vector k_r versus frequency.

To understand the generation mechanism of the GAMZFs, the squared cross-bicoherence [18], $b^2(f_1, f_2) = |B(f_1, f_2)|^2 / \left[\left\langle |v_r(f_1) v_\theta(f_2)|^2 \right\rangle \left\langle |\phi_f(f_1 + f_2)|^2 \right\rangle \right]$ of the perturbations is calculated. This is an indicator for the strength of nonlinear three-wave coupling. Here the bispectrum is described by $B(f_1, f_2) = \left\langle v_r(f_1) v_\theta(f_2) \phi_f^*(f_1 + f_2) \right\rangle$, with $v_r = (\phi_{f3} - \phi_{f2})/Bd_\theta$ and $v_\theta = E_{r1}/B$, while $\langle ... \rangle$ denotes an ensemble average and the number of ensemble realizations is N = 200. Figure 7 shows $b^2(f_1, f_2)$ values plotted in the region between the lines of the $f_1 = f_2$ and $f_1 = -f_2$ in the f_1 - f_2 plane for shot 4206. Positive and negative f_2 mean

the regions of the $f_1+|f_2|$ and $f_1-|f_2|$, respectively. The values of $b^2(f_1, f_2)$ at about $f_1-|f_2|\approx 7kHz$ and $f_2\approx\pm 7kHz$ are higher than the rest if the frequency is in the region $10<f_1<45$ kHz, indicating that the nonlinear three wave coupling is a plausible mechanism for the GAMZF generation. The frequency resolution is 1 kHz in this analysis, and signals are significantly above the noise level of 0.005 in the wide range of frequency.

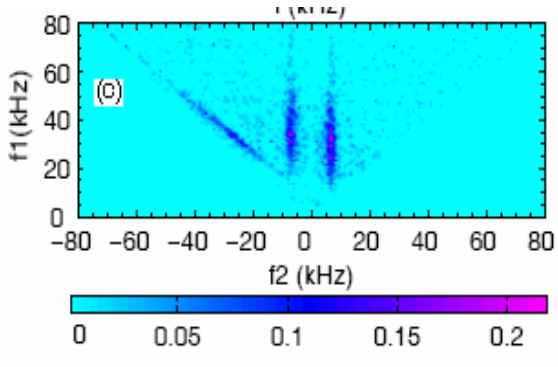

FIG. 7. The squared cross-bicoherence $b^2(f_1, f_2)$ plotted in the f_1- f_2 plane for shot 4206

The values of $b^2(f_1, f_2)$ at frequency $f_1-|f_2|\approx 7kHz$ and $f_2\approx\pm 7kHz$ are higher than the rest, indicating that the nonlinear three wave coupling is a plausible mechanism for the GAMZF creation.

The radial alignment error for the TSLP tips is about 1 mm in the ZF experiments, which can produce the comparable wave vector components in the poloidal and toroidal directions. The phase difference of the perturbations at two spatial points is able to describe as, $\Delta\phi = k_r r + k_\theta l_\theta + k_\varphi l_\varphi$. When the poloidal and toroidal wave vectors are zero, the error of poloidal wave number produced by radial alignment error of 1 mm is $\Delta k_\theta = k_r / 65$. Using the above k_r = 2.6 and 1.5 cm^{-1} with the GAMZFs, we obtain $\Delta k_\theta =$ 0.040 and 0.023 cm^{-1} for shots 4044 and 4206, respectively. Both are very close to the measurement values given above, $k_\theta = -0.05\pm 0.03$ and $k_\theta = -0.02\pm 0.01$ cm^{-1}. Therefore, the deviation of the measured poloidal wave numbers of the GAMZFs from the theoretically predicted *m = 0* symmetry may be attributed to the small radial alignment error. Similarly, when the poloidal and toroidal wave vectors are zero, the error of toroidal wave number produced by the radial alignment error of 1 mm is $\Delta k_\varphi = k_r / 800$. Using the above k_r = 2.6 cm^{-1} with the GAMZFs for shot 4044, we obtain $\Delta k_\varphi \approx$ 0.003 cm^{-1}, which is comparable with the measure value, $k_\phi = (0.2-0.4)\times 10^{-2}$ cm^{-1}. The connection line between tip 1 and 11 in shot 4044 is nearly parallel to the magnetic field line. There is a small angle between the connection line from tip 1 to 11 and the magnetic field line in shot 4026. The measurement value of toroidal wave vector in shot 4206 is much smaller that the estimation error of 0.002 cm^{-1}. Possible reason is due to the smaller radial alignment error. Therefore, the small difference of toroidal mode number from theoretic prediction (n = 0) may be reasonably explained by the probe alignment error as well.

5. Conclusion

A novel design of three-step Langmuir probe array has been successfully applied to study the zonal flows in the HL-2A tokamak. Three arrays are arranged at poloidal and toroidal directions to observe three-dimensional features of the zonal flows. Two arrays have poloidal separation of 6.5 cm; the third is separated toroidally by 80 cm, corresponding to poloidal and toroidal angles of 9.3 and 22.5 degrees. Two GAMZF discharges are analyzed with the safety factor 5.3 for shot 4044 and 3.5 for shot 4206, and line averaged density of (2 - 2.5)×10^{19} m^{-3}. The GAMZF frequencies are 9.3 kHz and 6.8 kHz for the two discharges. The FWHM at the GAMZF frequencies is 3-5 kHz, corresponding to the lifetime of 0.2-0.3 ms, which is over 20

times of the turbulent decorrelation time with an order of magnitude $\tau_d \sim 10\mu s$ during the zonal flow experiments.

The three dimensional features of the GAMZFs are simultaneously measured in the HL-2A tokamak. The radial wave vectors at the peak frequencies are estimated as $k_r = 2.6 \pm 0.2$ cm^{-1} for shot 4044 and $k_r = 1.5 \pm 0.2$ cm^{-1} for shot 4206, corresponding to the radial scale lengths of $\lambda = 2.4$ and 4.2 cm. The poloidal mode numbers estimated from their wave vectors of the GAMZFs are *m~1.8* and *m~0.7* for the two shots. The radial alignment error among the probe tips is ~1 mm. Using the above k_r = 2.6 and 1.5 cm^{-1} with the GAMZFs, the mode number errors produced by the radial alignment error of 1 mm are *m~1.5* and *0.85* for shots 4044 and 4206, respectively. Therefore, the deviation of the measured poloidal mode numbers of the GAMZFs from the theoretically predicted *m = 0* symmetry may be attributed to the small radial alignment error. The toroidal mode numbers are $n = 0.33 \pm 0.0.07 \sim 0$ and $n = 0.0 \pm 0.1 \sim 0$ along the magnetic field line for the two discharges, which are in good agreement with the theoretical prediction (n = 0). The squared cross-bicoherence of the turbulent perturbations for shot 4206 at the frequency $f_1 - |f_2| \approx 7kHz$ and $f_2 \approx \pm 7kHz$ are higher than the rest if the frequency is in the region *10<f_1< 45* kHz, indicating that the nonlinear three-wave coupling is a plausible mechanism for the GAMZF generation.

Acknowledgements

The suggestions from Profs. K. Itoh, A. Fujisawa, and H. Sanuki are gratefully acknowledged. The authors thank the HL-2A Team for the good operation of the machine. This work is partly supported by the National Natural Science Foundation of China, Grants No. 10135020, No. 10235010, No. 10575031, No. 10335060, and No. 10375020.

References

[1] Diamond, P. H., et al., Plasma Phys. Control. Fusion **47** (2005) R35.
[2] Lin, Z., et al., Science **281** (1998) 1835.
[3] Jakubowski, M., et al., Phys. Rev. Lett. **89** (2002) 265003.
[4] McKee, G.R., et al., Physics of Plasmas **10** (2003) 1712.
[5] McKee, G.R., et al., Plasma Phys. Control. Fusion **48** (2006) S123.
[6] Conway, G.D., et al., Plasma Phys. Control. Fusion **47** (2005) 1165.
[7] Nagashima, Y., et al., Phys. Rev. Lett. **95** (2005) 95002.
[8] Ido, T., et al., Plasma Phys. Control. Fusion **48** (2006) S41.
[9] Melnikov, A.V., et al., Plasma Phys. Control. Fusion **48** (2006) S87.
[10] Kraemer-Flecken, A., et al., Phys. Rev. Lett. **97** (2006) 045005.
[11] Xu, G.S., et al., Phys. Rev. Lett. **91** (2003) 125001.
[12] Shats, M.G., et al., Phys. Rev. Lett. **90** (2003) 125002.
[13] Fujisawa, A., et al., Phys. Rev. Lett. **93** (2004), 165002.
[14] Zhao, K.J., et al., Phys. Rev. Lett. **96** (2006), 255004.
[15] Yan, L.W., et al., Rev. Sci. Instru. **77 (2006),** (to be published).
[16] Yan, L.W., et al., Rev. Sci. Instru. **76** (2005) 093506.
[17] Liu, Y., et al., Nucl. Fusion **45** (2005) S239.
[18] Diamond, P. H., et al., Phys. Rev. Lett. **84** (2000) 4842.